Computers and Geotechnics 75 (2016) 48–56

Contents lists available at ScienceDirect

Computers and Geotechnics

journal homepage: www.elsevier.com/locate/compgeo

Research Paper

# Contact angle of soil minerals: A molecular dynamics study

Chao Zhang [a], Zhen Liu [a,*], Peng Deng [b]

[a] Department of Civil and Environmental Engineering, Michigan Technological University, Houghton, MI 49931, USA
[b] Department of Civil and Environmental Engineering, Colorado School of Mines, Golden, CO 80401, USA

ARTICLE INFO

*Article history:*
Received 29 June 2015
Received in revised form 15 January 2016
Accepted 17 January 2016
Available online 10 February 2016

*Keywords:*
Contact angle
Wettability
Molecular dynamics
Soil minerals
Unsaturated soil mechanics

ABSTRACT

In this paper, molecular dynamics was employed to study the wetting behavior of soil minerals. The basic concepts and methodologies of molecular dynamics were briefly summarized. A specific modeling and simulation procedure was presented to study the contact angles of solids using molecular dynamics. This procedure was employed to simulate the contact angles of three minerals, which are common in sand and silt fractions, i.e. α-quartz, orthoclase and muscovite. The simulated contact angle was 29° for α-quartz; 36° for orthoclase; and 116° for muscovite, which shows good agreement with the reported experimental or numerical results and thus substantiates the feasibility and accuracy of the proposed method. The simulation results also reveal that the contact angles of these minerals are considerably larger than zero and quite different from each other.

Published by Elsevier Ltd.

## 1. Introduction

Wettability of soil minerals is of critical importance in many aspects of geotechnical engineering, petroleum engineering, and soil science. Contact angle is a major indicator for wettability which could be measured experimentally. According to Young [1], the contact angle is a result of interfacial equilibrium and could be expressed as a function of interfacial surface tension. Fig. 1 schematically depicts the contact angle of the soil mineral–water–vapor interface $\theta$ where $\gamma_{SL}$, $\gamma_{SA}$ and $\gamma_{LA}$ denote the surface tension of soil mineral–water, soil mineral–vapor and water–vapor interfaces, respectively. In geotechnical engineering, the wettability of soils is a crucial element in formulating the Soil Water Characteristic Curve (SWCC), which is a fundamental concept in unsaturated soil mechanics [2,3]. Due to the high surface energy of soil minerals, for simplicity's sake, the contact angles of soil minerals are usually assumed to be constant (mostly zero) in unsaturated soil mechanics [4–6]. However, some recent experimental results revealed that these assumptions may be inappropriate for soil minerals [7]. In fact, the contact angle has been identified to be dependent on water potential, roughness, and temperature by soil scientists, agricultural engineers, and physical chemists [8–12]. Despite a few investigations into the effect of the contact angle [13], the effect of contact angles of soil minerals on the unsaturated soil behavior is far from being thoroughly understood. It is therefore indispensable to understand contact angles of soil minerals and quantify their effects on the unsaturated soil behavior.

The contact angle is measurable at the macroscopic scale while the surface tensions of solid–water and solid–vapor interfaces are difficult to be directly measured via experimental techniques [14]. According to Young's equation [1], the solid surface tensions could be obtained by measuring the contact angle experimentally [14]. In recent years, various experimental methods have been proposed to measure the surface tensions of the soil mineral–water system [15], for example, the capillary rise method [16], the sessile drop method [17] and Wilhelmy plate method [18]. As illustrated before, the contact angle may be affected by various factors, such as, roughness, temperature, heterogeneity, particle size and shape [19], which still needs a long-term further research to investigate. As a result, for one soil mineral, the contact angles measured by different researchers or different experimental methods usually exhibit discrepancies [20,21]. However, a thorough experimental research quantifying these effects on the contact angles of minerals is still absent [19]. The possible reason for this is that, to date, there is no efficient experimental or numerical tool capable of quantifying these factors.

Molecular Dynamics (MD) simulation has been recognized as an efficient tool to investigate the complex physical mechanisms at the molecular scale. The physical nature of the surface energy is dominated by crystallographic orientation of the solid surface [22]. Therefore, molecular dynamics simulation is by nature an efficient approach to study the contact angle of materials. In recent years, molecular dynamics simulations have been implemented to

* Corresponding author. Tel.: +1 906 487 1826.
*E-mail address:* zhenl@mtu.edu (Z. Liu).

http://dx.doi.org/10.1016/j.compgeo.2016.01.012
0266-352X/Published by Elsevier Ltd.

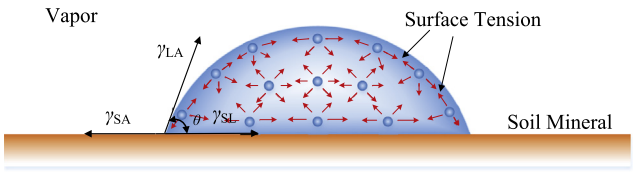


**Fig. 1.** Schematic diagram of contact angle of soil mineral–water–vapor system.

study the wetting behavior of some specific materials by materials scientists and chemists. Yuan and Zhao [23,24] studied the dynamic wetting, electrowetting and wetting on flexible hydrophilic pillar-arrays by means of molecular dynamics simulations. Werder et al. [25] studied the contact angles of carbon nanotubes through parallel molecular dynamics simulations. In their model, the simulated system was divided into three parts: water–water interaction, carbon nanotubes, and carbon–water interaction. In particular, the carbon–water interaction was modeled as Lennard–Jones interaction where the parameters need to be calibrated with reference to experimental data. Hong et al. [26] investigated the static and dynamic behavior of contact angles of a solid surface using molecular dynamics simulations. They pointed out that the wetting behavior, i.e. hydrophobic or hydrophilic, of the simulated solid surface could be identified as the changes in water–solid interaction energies. Park et al. [27] studied the effect of the solid surface morphology on the contact angles. The random roughness was created by adjusting the distribution function of the solid surface. Yan et al. [28] introduced a solvent environment to a simulated system of contact angles. They found that the water–solvent interaction was an important factor to the wetting behavior of the solid surface.

In contrast with the wide application of molecular dynamics to the contact angle study of graphite and carbon nanotubes, there is a very limited number of molecular dynamics studies targeting at the contact angles of minerals. Šolc et al. [29] studied the wettability of kaolinite using molecular dynamics simulations. They found that the tetrahedral surface of kaolinite is typically hydrophobic with a simulated contact angle of 105°. Tenney and Cygan [30] investigated the carbon dioxide, brine and kaolinite interactions through molecular dynamics simulations and calculated the corresponding contact angles. Despite these few molecular dynamics studies from Šolc et al. [29] and Tenney and Cygan [30], the contact angles of soil minerals have not been extensively investigated using molecular dynamics simulations.

Other than soil wettability, molecular dynamics has been employed by some geotechnical researchers to study soil behaviors. Ichikawa et al. [31] proposed a unified molecular dynamics and homogenization analysis framework to investigate the seepage behavior of bentonite. This framework was later extended to study a series of the seepage, diffusion and consolidation problems of bentonite [32–35]. Song et al. [36] explored the bridging scales methods for geo-materials from the molecular scale, the particle scale to the continuum scale. Bourg and Sposito have explored the double layer structure and diffusion performance of smectite or smectite-rich porous media [37,38]. Katti et al. have employed molecular dynamics simulations to study the mechanical behaviors of clay minerals under various loading schemes [39–42]. Amarasinghe and Anandarajah have studied the influence of fabric variables on the clay interparticle capillary water and upscaled the simulation results to model the hysteresis of fine-grained soils [43,44].

To promote its application in the geotechnical engineering community, molecular dynamics simulations are adopted in this study to explore the wetting behavior of soil minerals. Some basic concepts and methodologies of molecular dynamics are introduced in Section 2. A specific simulation method is presented in Section 3 particularly for the contact angles of soil minerals. Based on the method, a series of molecular dynamics simulations are conducted to explore the contact angles of soil minerals. Three typical soil minerals that are common in sand and silt fractions are selected for this study. The wetting processes of these soil minerals are simulated and their contact angles are determined from the time-average density profiles of droplets. The underlying physical mechanisms of wetting processes and their implications on unsaturated soil mechanics are discussed further in detail.

## 2. Basic concepts and methodologies of molecular dynamics

Molecular dynamics has been proven to be an efficient tool for investigating material behavior at the nanoscale. Two main assumptions are typically made in classical molecular dynamics [45,46]: (1) molecules or atoms are described as a system of interacting points, whose motion is described dynamically with a vector of instantaneous positions and velocities, and the interaction between atoms has a strong dependence on the spatial orientation and distances between separate atoms and (2) neither the mass nor number of atoms in the system will be changeless during the simulation process.

### 2.1. Governing equations

Newton mechanics is the theoretical basis for classical molecular dynamics. The motion of atoms could be represented by Newton's second law [47]:

$$m_i \frac{\partial^2 \mathbf{r}_i}{\partial t^2} = \mathbf{F}_i = \sum_{\substack{j=1 \\ (i \neq j)}}^{N_a} \mathbf{f}_{ij}, \tag{1}$$

where $m_i$ is the mass of atom; $\mathbf{r}_i = (x_i, y_i, z_i)$ is the coordinate of atom $i$; $t$ is time; $\mathbf{F}_i$ is the total force applied on atom $i$; $\mathbf{f}_{ij}$ is the interaction force applied on atom $i$ by atom $j$, and is usually a function of the displacement between atom $i$ and atom $j$; $N_a$ is the number of atoms in the system.

A complex formulation of classical mechanics is required for complicated simulation systems. The Lagrangian or Hamiltonian formulation of classic mechanics is usually employed for this purpose. For example, the Lagrangian formulation of the molecular dynamics system could be written as [45]:

$$m_i \frac{\partial^2 \mathbf{r}_i}{\partial t^2} = -\frac{\partial U(\mathbf{r}_1, \mathbf{r}_2, \ldots, \mathbf{r}_{N_a})}{\partial \mathbf{r}_i} \equiv \mathbf{F}_i, \tag{2}$$

where $U$ represents the total potential energy of the system, which is a function of atomic coordinates.

### 2.2. Interatomic potentials

From Eqs. (1) and (2), it could be observed that the mechanical properties are mainly dominated by the expression of the interatomic force $\mathbf{f}_{ij}$ or the total potential energy $U$. In reality, the total potential energy of the system could be very complicated due to the presence of quantum effects. Therefore, in order to simulate the complex system with acceptable computational costs, the interatomic potentials should well consider the complicated quantum effects during the simulated mechanical process. In practice, for simplicity, the interatomic potentials are usually treated as pairwise interatomic potentials by assuming that the interatomic potential between two atoms is a function of the coordinates and physical properties of these two atoms, and independent of other atoms. The interatomic potential usually decays with the distance

between the atoms. According to the decaying velocity, the interatomic potentials could be classified as short-range potentials and long-range potentials.

#### 2.2.1. Short-range potentials

The van der Waals potential may be the most popular short-range potential in molecular dynamics. The van der Waals potential represents the interatomic forces between atoms caused by instantaneous dipoles or momentary polarization which is known as van der Waals forces [46]. Various mathematical functions have been proposed to describe the van der Waals potential. The Lennard–Jones (LJ) 12–6 potential is a mathematical function widely adopted for this potential:

$$U_{ij} = 4\varepsilon_{ij}\left[\left(\frac{\sigma_{ij}}{r_{ij}}\right)^{12} - \left(\frac{\sigma_{ij}}{r_{ij}}\right)^{6}\right], \tag{3}$$

where $\varepsilon_{ij}$ is the characteristic energy; $\sigma_{ij}$ is the distance corresponding to the minimal interaction energy; and $r_{ij}$ is the distance between atom $i$ and atom $j$. Fig. 2 schematically depicts a Lennard–Jones 12–6 potential of the Silicon–Oxygen interaction in the α-quartz according to the ClayFF force field [48], where the potential amplitude is normalized by $4\varepsilon_{ij}$. It could be observed that the potential decays rapidly with increasing distance between the atoms.

#### 2.2.2. Long-range potentials

A typical long-range potential is the Coulomb potential which decays slowly with the distance between particles. The Coulomb potential represents the electrostatic interaction between point charges. The mathematical function for the Coulomb potential could be expressed as:

$$U_{ij} = \frac{e^2}{4\pi\epsilon_0}\frac{q_i q_j}{r_{ij}}, \tag{4}$$

where $q_i$ and $q_j$ are the partial charges of atom $i$ and $j$, respectively; $\epsilon_0$ is the dielectric permittivity of the vacuum; $e$ is the charge of an electron; $r_{ij}$ is the distance between atom $i$ and atom $j$. Fig. 2 schematically depicts a Coulomb potential of the Silicon–Oxygen interaction in the α-quartz according to the ClayFF force field [48], where the potential amplitude is normalized by $e^2/(4\pi\epsilon_0)$. It could be observed that, compared to Lennard–Jones 12–6 potential, the decaying velocity of the Coulomb potential is remarkably lower.

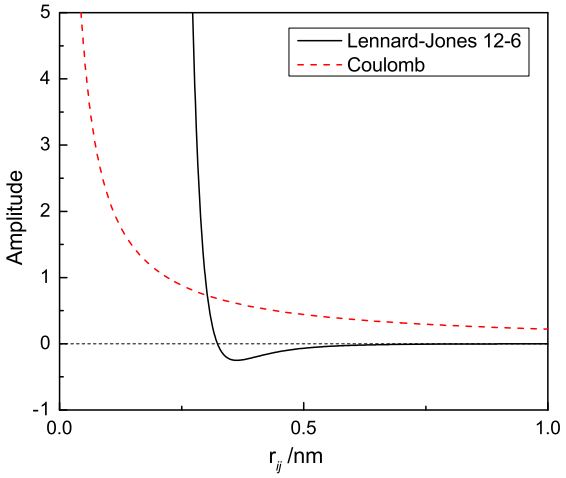


**Fig. 2.** Lennard–Jones 12–6 potential and Coulomb potential of the Silicon–Oxygen interaction in the α-quartz.

### 2.3. Numerical treatment of interatomic potentials

High computational costs are a major stumbling block to the wide application of molecular dynamics simulations. Therefore, it is of critical importance to tackle the calculation of interatomic potentials with reasonable accuracy and acceptable computational costs.

#### 2.3.1. Truncation method

Strictly speaking, atoms will interact with each other no matter how far they are from each other. Short-range potentials decay rapidly with the increasing distance $r_{ij}$. Thus, it is reasonable to define a cutoff radius $r_c$ to truncate infinite potentials into finite potentials. As for atom $i$, only its interactions with the atoms within a distance of $r_c$ need to be taken into consideration. For example, the truncated Lennard–Jones 12–6 potential could be rewritten as [47]:

$$U_{ij} = \begin{cases} 4\varepsilon_{ij}\left[\left(\frac{\sigma_{ij}}{r_{ij}}\right)^{12} - \left(\frac{\sigma_{ij}}{r_{ij}}\right)^{6}\right]; & r_{ij} < r_c \\ 0; & r_{ij} \geqslant r_c \end{cases}. \tag{5}$$

#### 2.3.2. Ewald summation method

In contrast to short-range potentials, long-range force effects need to be considered for the Coulomb potentials. Notwithstanding, it is not feasible to calculate the long-range potentials directly due to unacceptable computational costs. Various approximation methods have been proposed to deal with the long-range potentials. The Ewald summation method is a widely adopted approximation method which reorganizes the potentials into a particular form that could be easily evaluated [47]. Rapaport [47] has made an excellent introduction to this method. In this study, a Fourier-based Ewald summation method called Particle–Particle, Particle-Mesh (PPPM) method [49] was adopted to calculate long-range Coulomb forces.

## 3. MD model for the simulation of contact angle

### 3.1. Molecular structures

Quartz, feldspar and mica are the most common minerals in sand and silt fractions of soils [50]. Their physical properties dominate the engineering behavior of non-cohesive soils. However, to the authors' best knowledge, there are only a few studies aiming at the wetting behavior of quartz while there is no research addressing the contact angles of feldspar and mica using molecular dynamics simulations. In this study, the contact angles of one type of quartz (α-quartz), feldspar (orthoclase) and mica (muscovite) were selected and simulated by using molecular dynamics. The crystal structures of these soil minerals are well known [51–53], whose lattice parameters and corresponding references are summarized in Table 1.

### 3.2. Interatomic force fields of soil minerals

In a molecular dynamics system, there exists various types of interatomic potentials. It is necessary to define a force field to calculate these interatomic potentials in the system mathematically. A force field is a set of functions and parameters defined to calculate these interatomic potentials. In recent years, various force fields have been proposed for the molecular modeling of water and minerals. The aim of the current study is to investigate the soil mineral–water system. In this system, three types of interatomic interactions need to be taken into consideration: the soil

**Table 1**
Lattice parameters and corresponding references of the soil minerals selected for MD simulations.

| Mineral | Chemical formula | Lattice parameters | | | | | | References |
|---|---|---|---|---|---|---|---|---|
| | | $a$ (Å) | $b$ (Å) | $c$ (Å) | $\alpha$ (°) | $\beta$ (°) | $\gamma$ (°) | |
| α-Quartz | $SiO_2$ | 4.916 | 4.916 | 5.405 | 90 | 90 | 120 | [51] |
| Orthoclase | $KSi_3Al_3O_{12}H_2$ | 8.544 | 13.03 | 7.195 | 90 | 115.68 | 90 | [52] |
| Muscovite | $KSi_3AlO_8$ | 5.199 | 9.027 | 20.106 | 90 | 95.782 | 90 | [53] |

mineral–soil mineral interaction, the soil mineral–water interaction, and the water–water interaction.

In terms of the soil mineral–soil mineral interaction, the total interatomic potential $U_{total}$ is expressed as a combination of the Coulomb interaction $U_{Coul}$ and van der Waals interaction $U_{vdW}$:

$$U_{total} = U_{Coul} + U_{vdW}. \tag{6}$$

The total Coulomb interaction energy could be represented by a summation form of Eq. (4) as

$$U_{Coul} = \frac{e^2}{4\pi\epsilon_0}\sum_{i\neq j}\frac{q_i q_j}{r_{ij}}, \tag{7}$$

where $q_i$ and $q_j$ are the partial charges of atom $i$ and $j$, respectively; $\epsilon_0$ is the dielectric permittivity of the vacuum; $e$ is the charge of the electron; and $r_{ij}$ is the distance between atom $i$ and atom $j$. The van der Waals interaction energy is formulated in a summation form as Eq. (3):

$$U_{vdW} = \sum_{i\neq j} 4\varepsilon_{ij}\left[\left(\frac{\sigma_{ij}}{r_{ij}}\right)^{12} - \left(\frac{\sigma_{ij}}{r_{ij}}\right)^{6}\right], \tag{8}$$

where $\varepsilon_{ij}$ is the characteristic energy and $\sigma_{ij}$ is the distance corresponding to the minimal interaction energy. The values of $\varepsilon_{ij}$ and $\sigma_{ij}$ could be determined empirically. For this purpose, quite different values have been proposed [48,54]. The ClayFF force field is a general force field for clay minerals developed by Cygan et al. [48]. In the ClayFF force field, the soil mineral–soil mineral interaction and the soil mineral–water interaction are modeled as nonbonded interactions while the water–water interaction is modeled by the SPC/E water model. The nonbonded interaction potential is expressed as a combination of Coulomb interaction and van der Waals interaction whose mathematical formulations are identical to Eqs. (6)–(8). Skelton and Fenter [55] investigated the performance of some existing force fields for simulating the quartz–water interface via the comparison with the results of ab initio molecular dynamics (AIMD) and X-ray analysis. They concluded that the ClayFF force field is suitable for the modeling of complex quartz–aqueous systems. Kerisit et al. [56] made some modifications to the parameters of the ClayFF force field to simulate feldspars. Teich-McGoldrick et al. [57] studied the elastic and structural properties of muscovite by the ClayFF force field. Given its successful applications in simulating quartz, orthoclase and muscovite, the values of $\varepsilon_{ij}$, $\sigma_{ij}$, $q_i$ and $q_j$ were adopted from the ClayFF force field [48] and the modified ClayFF force field [56] in this study. For the interactions between different atomic species $i$ and $j$, the values of $\varepsilon_{ij}$ and $\sigma_{ij}$ could be calculated according to Lorentz–Bertholet mixing rule as [58]

$$\varepsilon_{ij} = \sqrt{\varepsilon_i\varepsilon_j}; \quad \sigma_{ij} = \frac{1}{2}(\sigma_i + \sigma_j). \tag{9}$$

In terms of the water–water interaction, various water models have been proposed, for example, the simple point charge (SPC) model [59], the extended simple point charge (SPC/E) model [60], the 3-point transferable intermolecular potential (TIP3P) model and the 4-point transferable intermolecular potential (TIP4P) model [61]. Šolc et al. [29] conducted a series of contact angle simulations for kaolinite by using different water models and different amount of water molecules, which revealed that the contact angle could be well reproduced by these different simulation cases. The SPC/E model was employed in this study to be compatible with the ClayFF force field.

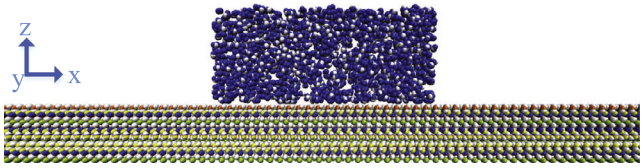


**Fig. 3.** Initial configuration of the simulated soil mineral–water system.

### 3.3. Initial configuration

As illustrated in Fig. 3, the initial soil mineral–water system was modeled as a body of water placed on the top of a soil mineral slab. The bulk water was placed 3.1 Å above the soil mineral slab. The simulation cell size was about $400 \times 20 \times 200$ Å$^3$ and adjusted to be integer multiples of the lattice constants (for example, the lattice parameters $a$, $b$ and $c$ provided in Table 1).

The initial configurations of soil mineral slabs were generated by stacking the mineral crystal unit cell along $x$-, $y$- and $z$- directions. In this study, the dimensions of soil mineral slabs were set as about $400 \times 20 \times 30$ Å$^3$ and then adjusted to be integer multiples of the lattice constants. The initial configuration of the α-quartz slab could be smoothly obtained by following this process. However, due to the presence of isomorphous substitution, this process is more complex for orthoclase and muscovite. Isomorphous substitution is the replacement of ions of one kind by another kind without changing the crystal structures [50]. As a result, some crystallographic sites of soil minerals are partially occupied by multiple types of ions. In this study, isomorphous substitutions were assumed to be uniformly distributed along soil mineral slabs when generating the initial configurations of orthoclase and muscovite.

The initial configuration of the water needs to be carefully treated. A bad initial configuration of the water can easily cause simulation errors. The distances between water molecules should maintain a value around 3.1 Å to obtain a good initial configuration. It should be noted that water molecules in the periodic cells also need to be taken into consideration. In this study, the initial configuration of the bulk water was generated as a rectangular cuboid droplet using Packing Optimization for Molecular Dynamics Simulations (PACKMOL). PACKMOL [62] is an open-source package developed for generating good initial configurations without disrupting simulations. The dimensions of the rectangular cuboid in $x$- and $z$-directions are 60 Å. The dimension of the rectangular cuboid in $y$-direction is 3.1 Å shorter than that of soil mineral slabs to avoid an excessively short distance between water molecules and mineral atoms. The number of water molecules filled in the rectangular cuboid was calculated to make the initial density of the bulk water equal to that of liquid water.

### 3.4. Simulation setup

In MD simulations, the periodic boundary condition is usually adopted to eliminate the so called surface effects [45]. In this study,

the boundary conditions in the $x$- and $y$-directions, i.e. parallel to the soil mineral slab, were set as periodic boundaries, while the boundary in $z$-direction, i.e. normal to the mineral layer was fixed to omit the interactions between image cells along the $z$-direction. Two reflecting walls were placed on the top and bottom of the simulation cell, respectively, to prevent the loss of water molecules through these two boundaries by a LAMMPS command "wall/reflect". Due to the periodic boundaries in the $y$-direction, the droplet could be regarded as infinitely long. Therefore, the simulated soil mineral–water system could be regarded as a typical 2-dimensional system. According to Tenney and Cygan [30], the adoption of this type of 2-dimensional simulation system has the potential to reduce the scale effects by decreasing droplet curvatures and eliminating three-phase line tensions. In terms of the capillary water in soils, the gravitational gradient has small influence on the geometry of meniscus [63] especially for the nanoparticles [64]. Therefore, the gravity was neglected in the current simulations as suggested by Tenney and Cygan [30].

Molecular dynamics simulation is a well-developed numerical tool for materials and chemistry research. There are many commercial and open source software packages available for molecular dynamics simulations. The Large-scale Atomic/Molecular Massively Parallel Simulator (LAMMPS) [65,66] distributed by the Sandia National Laboratories is an open-source package for classic molecular dynamics simulations, and has been widely adopted for simulating complex material behavior. In this study, all the molecular dynamics simulations were conducted with LAMMPS and visualized with Visual Molecular Dynamics (VMD) [67]. The simulated soil mineral–water system was performed under the NVT ensemble (constant number, volume and temperature) with a temperature of 300 K. The LJ 12–6 interactions were truncated to 12 Å, i.e. $r_c = 12$ Å, while the long-range Columbic forces were calculated by the PPPM method [49] with 99.99% accuracy. Since the boundary conditions of the simulation cell were fixed in the $z$-direction, a command "slab" in LAMMPS was employed to enable the PPPM calculation. All the solid atoms were fixed to accelerate the simulations. Water molecules were kept rigid by using the SHAKE algorithm [68] to reduce computational costs during the simulations. Newton's equations of motion were integrated with a 1.0 fs time step. The simulations were performed for 3 ns. The molecular trajectories during the last 2 ns were recorded to calculate time average density profiles which will be used to determine the contact angle.

## 4. Results and discussions

### 4.1. Simulation results of the soil mineral–water systems

In general, soil minerals have several cleavage surfaces. For simplicity, only the (001) cleavage surfaces were considered in this study. A water droplet was placed on the (001) cleavage surface of α-quartz, orthoclase and muscovite. The simulated process lasted for 3 ns. If the total potential energy maintains fluctuating around a certain value for a long simulation time, the soil mineral–water systems were believed to have reached an equilibrium state. The equilibrium state is a statistical definition in molecular dynamics. That is, even though the simulated system reaches the equilibrium state, water molecules still move fast and the shape of the droplets will change at every step.

Fig. 4 shows the front views of the simulated systems in the equilibrium state for α-quartz, orthoclase and muscovite, respectively. As can be seen, although the shapes of the water droplets could be regarded as rounded, the water droplets are not ideally symmetrical, which is consistent with our assumption that the simulated system is in a statistically equilibrium state. Apart from the water droplets, some separate water molecules were absorbed

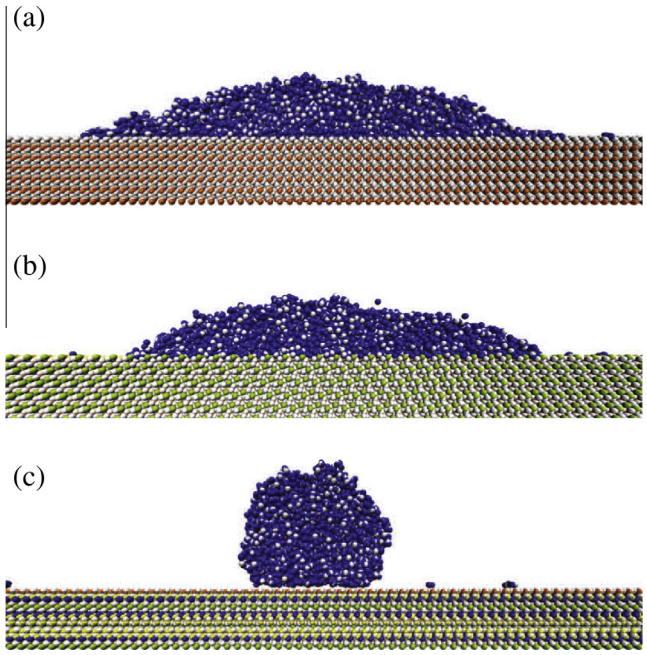


**Fig. 4.** Snapshots of soil mineral–water systems at the equilibrium state for: (a) α-quartz; (b) orthoclase; and (c) muscovite.

on the soil mineral surfaces. This phenomenon could be explained by the molecular exchange between the water droplets and vapor. During the simulation processes, some water molecules escaped from the bulk water into the vapor, while simultaneously, some water molecules in the vapor were adsorbed to the soil mineral surface. Compared with α-quartz and orthoclase, the contact area between muscovite and the water droplet is smaller. It means that the surface energy of the (001) cleavage surface of muscovite is lower than that of α-quartz and orthoclase. Based on the instantaneous water droplet shape illustrated in Fig. 4, the (001) cleavage surfaces of α-quartz and orthoclase can be claimed to be hydrophilic whereas the muscovite can be claimed to be hydrophobic.

Because the soil mineral–water system maintains a statistical equilibrium, time average density profiles of water molecules were used to interpret the simulation results. As described in Section 3.4, the molecular trajectories in the last 2 ns were recorded to determine time average density profiles. Considering that the simulations were 2-dimensional, a bin size of $0.5 \times 0.5$ Å$^2$ was employed to calculate the time average density profiles. As illustrated in Figs. 5–7, the time average density profiles of water droplets were calculated using the molecular trajectories recorded in the last 2 ns to quantify the wetting behavior of these soil minerals. It can be observed that a rounded water droplet shape can be easily identified from the time average density profiles. But it is also interesting to mention that the observed water droplets are not perfectly homogenous and continuous, and there exists a remarkable isolated layer at the bottom of the water droplet. This monomolecular layer should be attributed to the presence of the precursor film (PF). Yuan and Zhao [23] observed that the water molecules in the PF layer were well-ordered. For example, in Figs. 5 and 6, the PF layer was composed of a series of well-ordered points. The water molecules in the PF layer tended to stay in the potential wells between the surface mineral atoms, which is consistent with the observation of Yuan and Zhao [23].

### 4.2. Determination of contact angles

In this study, contact angles were measured from the density profiles of water molecules. For this purpose, we need to extract

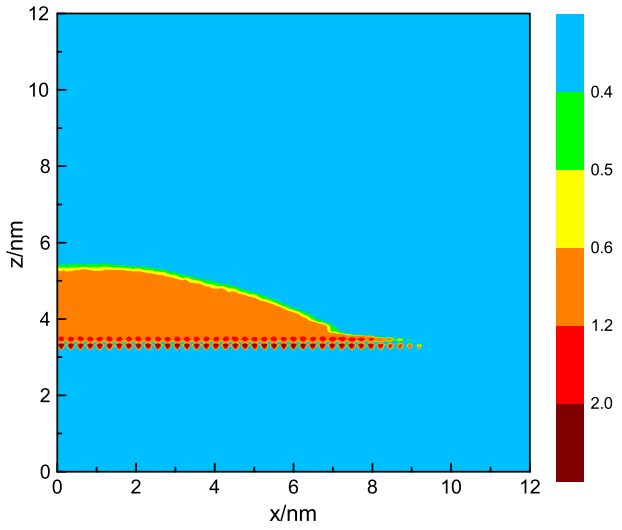


**Fig. 5.** Time average density profile (in g cm$^{-2}$) of a water droplet on α-quartz.

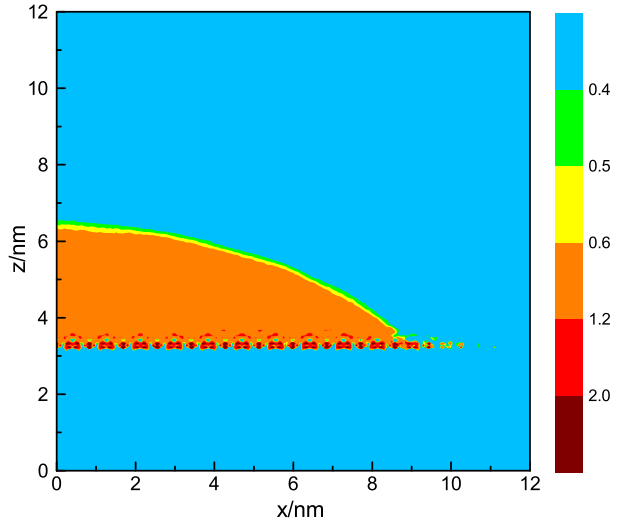


**Fig. 6.** Time average density profile (in g cm$^{-2}$) of a water droplet on orthoclase.

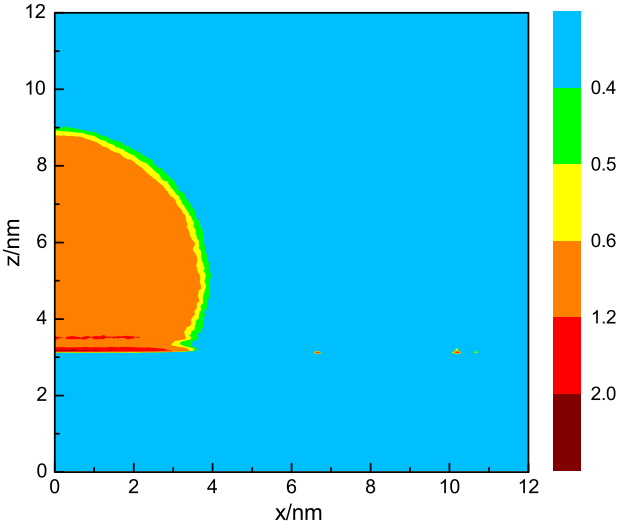


**Fig. 7.** Time average density profile (in g cm$^{-2}$) of a water droplet on muscovite.

the boundary between liquid water and vapor from the time average density profiles. The density distribution across the transient region between the liquid water and vapor could be expressed as [26,29]

$$\rho(z) = \frac{1}{2}(\rho^l + \rho^v) - \frac{1}{2}(\rho^l - \rho^v)\tanh\left(\frac{2(z - z_e)}{d}\right), \tag{10}$$

where $\rho^l$ is the density of liquid water; $\rho^v$ is the density of vapor; $z_e$ is the $z$-coordinate of the center of the transition region; and $d$ is the thickness of the transition region. For simplicity, Eq. (10) could be rewritten as follows by assuming the density of vaporis zero:

$$\rho(z) = \frac{1}{2}\rho^l\left[1 - \tanh\left(\frac{2(z - z_e)}{d}\right)\right]. \tag{11}$$

In this equation, the variables $\rho^l$, $z_e$ and $d$ are unknown, which can be determined by least-squares fitting to measured density profile data. At a certain $x$-coordinate $(x_i)$, there are many bins along the $z$-direction. The density profile data of these bins were fitted with Eq. (11) to obtain the density distribution function along the $z$-direction at this $x$-coordinate. The water density at the boundary between liquid water and vapor is assumed to be 0.5 g cm$^{-2}$. Then the $z$-coordinate at the water droplet's boundary $(z_i)$ could be easily calculated by the obtained density distribution equation. By repeating this procedure, a series of the coordinates $(x_i, z_i)$ along the droplet boundary could be obtained. It should be noted that, in order to obtain enough data for the droplet boundary, the curve fittings for hydrophilic cases $(\theta < 90^\circ)$ were conducted along the $x$-direction while those for hydrophobic cases $(\theta \geqslant 90^\circ)$ were conducted along the $z$-direction. Figs. 8–10 illustrate density profiles (scatter line) along the centerline of the water droplets and corresponding fitted density distribution functions (solid line) for α-quartz, orthoclase and muscovite, respectively. It is seen that the fitting functions could well approximate the transition region between the water droplet and vapor. The water molecule density profiles intensively fluctuate near the soil mineral surface, which is consistent with the observation of the PF layer.

The water droplet is assumed to be perfectly rounded. Accordingly, the mathematical equation of circles could be expressed as

$$(x - a)^2 + (z - b)^2 = R^2, \tag{12}$$

where $a$ and $b$ are the $x$-and $z$-coordinates at the center of the circle, respectively; $R$ is the radius of the circle. The values of $a$, $b$ and $R$ could be determined by another least-square fitting process with

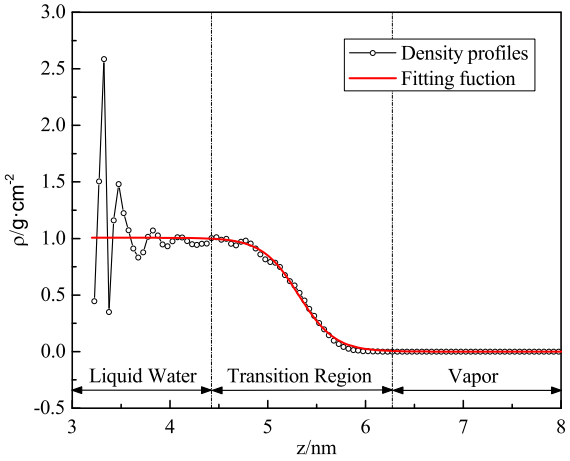


**Fig. 8.** Density profile along the centerline of the water droplet on α-quartz and corresponding density distribution function.

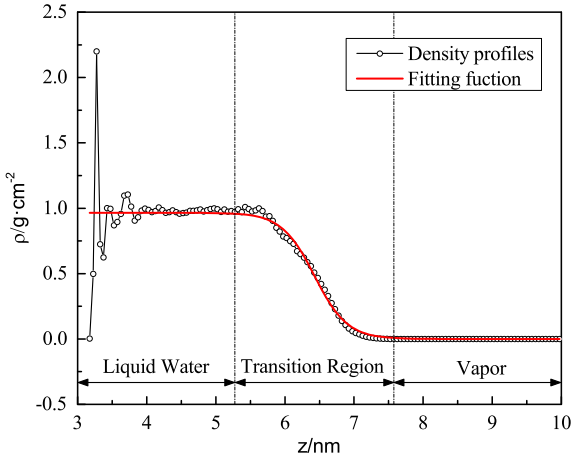


**Fig. 9.** Density profile along the centerline of the water droplet on orthoclase and corresponding density distribution function.

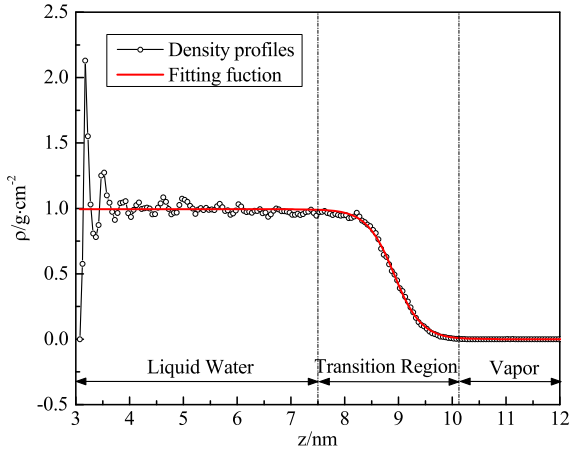


**Fig. 10.** Density profile along the centerline of the water droplet on muscovite and corresponding density distribution function.

Eq. (12) to the obtained coordinates $(x_i, z_i)$ along the droplet boundary. The $z$-coordinate at the top of the solid slab is assumed to be $z_a$. Therefore, the contact angle could be calculated as

$$\theta = \arccos\left(\frac{z_a - b}{R}\right). \tag{13}$$

Figs. 11–13 illustrate the determinations of the contact angles of α-quartz, orthoclase and muscovite, respectively. The dashed straight line, solid straight line and solid curve represent mineral surface, tangent line and fitting circle, respectively, while the red dots represent the coordinates $(x_i, z_i)$ along the water droplet boundary. In order to obtain enough data for determination of contact angles, the function fitting processes of α-quartz and orthoclase were conducted along the $z$-direction whereas that of muscovite were conducted along the $x$-direction.

### 4.3. Calculated contact angles of soil minerals

As summarized in Table 2, the computed contact angles are approximately 29°, 36° and 116° for the (001) cleavage surfaces of α-quartz, orthoclase and muscovite, respectively. The contact angle of α-quartz measured by Szyszka [69] using spherical particles immersion method is 31°, which is in good agreement with the computed contact angle of present study, i.e. 29°. In terms of orthoclase, the simulated contact angle value of 36° is very comparable

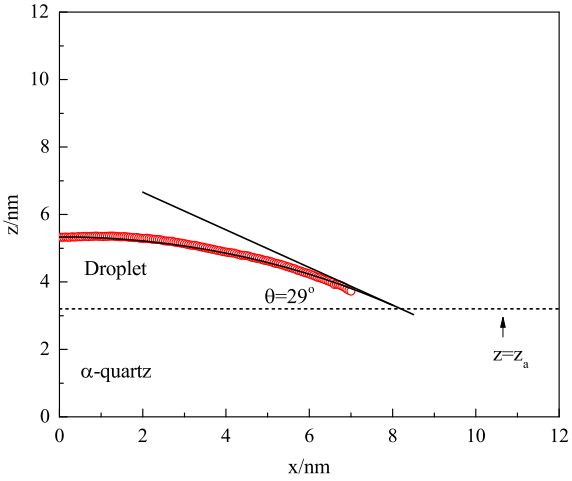


**Fig. 11.** Determination of the contact angle of α-quartz.

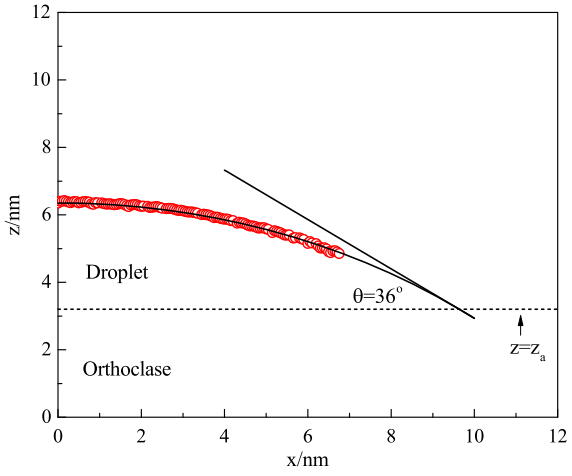


**Fig. 12.** Determination of the contact angle of orthoclase.

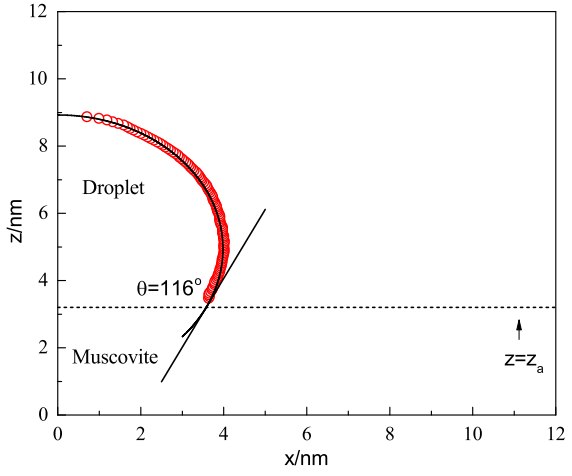


**Fig. 13.** Determination of the contact angle of muscovite.

to the experimental results from Karagüzel et al. [70], i.e. 45°, while for muscovite, the simulated contact angle on its (001) cleavage surface is consistent with the observations for kaolinite by Šolc et al. [29]. These consistences with existing research observations confirm the great potential of molecular dynamics for simulating soil mineral–water interfacial interactions.

**Table 2**
Computed contact angles for α-quartz, orthoclase and muscovite.

| Mineral | Cleavage surface | Contact angle (°) |
|---|---|---|
| α-Quartz | (001) | 29 |
| Orthoclase | (001) | 36 |
| Muscovite | (001) | 116 |

The soil–water interfacial interaction and the pore size distribution are two main elements in the SWCC. Compared with the extensive research on the pore size distribution, there are very limited research directed to understanding water soil interfacial interaction. The contact angles of soil minerals are usually assumed to be constant (mostly zero) in the existing research [4–6]. However, in this preliminary study, the computed contact angles vary intensively for different soil minerals, and the contact angle of the (001) cleavage surface of muscovite is hydrophobic, which contradicts the constant (mostly zero) contact angle assumption. Therefore, the validity of this assumption and the water soil interfacial interaction still need to be comprehensively investigated. Considering the difficulties in experimentally measuring the contact angles of soils, molecular dynamics simulation can possibly be developed into an effective tool in investigating the complex soil–water interfacial interactions at the scale where the interactions occur.

## 5. Summary and conclusions

This study aims at introducing the molecular dynamics to the geotechnical engineering community as a simulation technique to investigate the wetting behavior of soil minerals. The basic concepts and theoretical basis for this method were firstly introduced. A specific molecular dynamics modeling simulation procedure was proposed for the contact angle studies of soil minerals. In particular, the contact angles of the (001) cleavage surface of α-quartz, orthoclase and muscovite were simulated using the proposed method. It was observed that the contact angles vary intensively with soil mineral types and the contact angle of the (001) cleavage surface of these soil minerals were remarkably larger than zero, which contradicts the constant (mostly zero) contact angle assumption. The computed contact angles of soil minerals are consistent with the existing experimental observations, which validates the feasibility of the proposed method. It should be noted that the contact angle may be influenced by many factors such as temperature, surface roughness and cleavage surface, which needs a long-term further research.

The primary mission of this current study is to introduce molecular dynamics simulations to investigate the wetting behavior of soil minerals in geotechnical engineering community. In terms of unsaturated soil mechanics research, the water soil interfacial interaction is far from being well understood. Molecular dynamics simulation shows great potential to stimulate the research in this field. It is expected that molecular dynamics simulations will help improve the understanding of macroscopic soil behavior at the nanoscale level and fill some existing knowledge gaps in geotechnical engineering field, such as liquid bridge force between soil particles, double layer repulsive force, and ice nucleation in soils.

## Acknowledgements

The financial support from the Michigan Space Grant Consortium is gratefully acknowledged. We also acknowledge Superior, a high performance computing cluster at Michigan Technological University, for providing computational resources to fulfill this study. The insightful and constructive comments provided by the anonymous reviewers are appreciated by the authors.

## References

[1] Young T. An essay on the cohesion of fluids. Philos Trans Roy Soc Lond 1805:65–87.
[2] Fredlund DG, Rahardjo H. Soil mechanics for unsaturated soils. John Wiley & Sons; 1993 [ISBN 047185008X].
[3] Lu N, Likos WJ. Unsaturated soil mechanics. John Wiley & Sons; 2004 [ISBN 0471447315].
[4] Arya LM, Paris JF. A physicoempirical model to predict the soil-moisture characteristic from particle-size distribution and bulk-density data. Soil Sci Soc Am J 1981;45(6):1023–30.
[5] Bachmann J, van der Ploeg RR. A review on recent developments in soil water retention theory: interfacial tension and temperature effects. J Plant Nutr Soil Sci 2002;165(4):468–78. http://dx.doi.org/10.1002/1522-2624(200208)165:4<468::Aid-Jpln468>3.0.Co;2-G.
[6] Fredlund DG, Xing AQ, Huang SY. Predicting the permeability function for unsaturated soils using the soil–water characteristic curve. Can Geotech J 1994;31(4):533–46.
[7] Liu Z, Yu X, Wan L. Capillary rise method for the measurement of the contact angle of soils. Acta Geotech 2014:1–15.
[8] Drelich J, Miller JD. The effect of solid-surface heterogeneity and roughness on the contact-angle drop (bubble) size relationship. J Colloid Interface Sci 1994;164(1):252–9.
[9] Goebel MO, Bachmann J, Woche SK, Fischer WR, Horton R. Water potential and aggregate size effects on contact angle and surface energy. Soil Sci Soc Am J 2004;68(2):383–93.
[10] Grant SA, Bachmann J. Effect of temperature on capillary pressure. Geophys Monograph 2002;129:199–212.
[11] Quéré D. Wetting and roughness. Annu Rev Mater Sci 2008;38:71–99.
[12] Ramírez-Flores JC, Woche SK, Bachmann J, Goebel MO, Hallett PD. Comparing capillary rise contact angles of soil aggregates and homogenized soil. Geoderma 2008;146(1):336–43.
[13] Likos WJ, Lu N. Hysteresis of capillary stress in unsaturated granular soil. J Eng Mech 2004;130(6):646–55. http://dx.doi.org/10.1061/(Asce)0733-9399(2004)130:6(646).
[14] Kwok DY, Lam CNC, Li A, Leung A, Wu R, Mok E, et al. Measuring and interpreting contact angles: a complex issue. Colloids Surf A – Physicochem Eng Aspects 1998;142(2–3):219–35. http://dx.doi.org/10.1016/S0927-7757(98)00354-9.
[15] Chau T. A review of techniques for measurement of contact angles and their applicability on mineral surfaces. Miner Eng 2009;22(3):213–9.
[16] Adamson A, Gast A. Physical chemistry of surfaces. John Wiley & Sons; 1997 [ISBN 9780471148739].
[17] Bachmann J, Horton R, Ploeg RRVD, Woche S. Modified sessile drop method for assessing initial soilwater contact angle of sandy soil. Soil Sci Soc Am J 2000;64(2):564–7.
[18] Bachmann J, Woche SK, Goebel MO, Kirkham MB, Horton R. Extended methodology for determining wetting properties of porous media. Water Resour Res 2003;39(12).
[19] Chau TT, Bruckard WJ, Koh PT, Nguyen AV. A review of factors that affect contact angle and implications for flotation practice. Adv Colloid Interface Sci 2009;150(2):106–15.
[20] Erbil HY, McHale G, Rowan S, Newton M. Determination of the receding contact angle of sessile drops on polymer surfaces by evaporation. Langmuir 1999;15(21):7378–85.
[21] Shang J, Flury M, Harsh JB, Zollars RL. Comparison of different methods to measure contact angles of soil colloids. J Colloid Interface Sci 2008;328(2):299–307.
[22] Chawla K. Composite materials: science and engineering. Springer; 2012 [ISBN 9780387743653].
[23] Yuan Q, Zhao YP. Precursor film in dynamic wetting, electrowetting, and electro-elasto-capillarity. Phys Rev Lett 2010;104(24):4. http://dx.doi.org/10.1103/PhysRevLett.104.246101.
[24] Yuan Q, Zhao YP. Wetting on flexible hydrophilic pillar-arrays. Sci Rep 2013;3:1944. http://dx.doi.org/10.1038/srep01944.
[25] Werder T, Walther JH, Jaffe RL, Halicioglu T, Noca F, Koumoutsakos P. Molecular dynamics simulation of contact angles of water droplets in carbon nanotubes. Nano Lett 2001;1(12):697–702. http://dx.doi.org/10.1021/Nl015640u.
[26] Hong SD, Ha MY, Balachandar S. Static and dynamic contact angles of water droplet on a solid surface using molecular dynamics simulation. J Colloid Interface Sci 2009;339(1):187–95.
[27] Park JY, Ha MY, Choi HJ, Hong SD, Yoon HS. A study on the contact angles of a water droplet on smooth and rough solid surfaces. J Mech Sci Technol 2011;25(2):323–32. http://dx.doi.org/10.1007/s12206-010-1218-2.
[28] Yan MQ, Yang XN, Lu YJ. Wetting behavior of water droplet on solid surfaces in solvent environment: a molecular simulation study. Colloids Surf A – Physicochem Eng Aspects 2013;429:142–8. http://dx.doi.org/10.1016/j.colsurfa.2013.03.067.
[29] Šolc R, Gerzabek MH, Lischka H, Tunega D. Wettability of kaolinite (001) surfaces molecular dynamic study. Geoderma 2011;169:47–54. http://dx.doi.org/10.1016/j.geoderma.2011.02.004.

[30] Tenney CM, Cygan RT. Molecular simulation of carbon dioxide, brine, and clay mineral interactions and determination of contact angles. Environ Sci Technol 2014;48(3):2035–42. http://dx.doi.org/10.1021/es404075k.
[31] Ichikawa Y, Kawamura K, Nakano M, Kitayama K, Kawamura H. Unified molecular dynamics and homogenization analysis for bentonite behavior: current results and future possibilities. Eng Geol 1999;54(1–2):21–31. http://dx.doi.org/10.1016/S0013-7952(99)00058-7.
[32] Ichikawa Y, Kawamura K, Nakano M, Kitayama K, Seiki T, Theramast N. Seepage and consolidation of bentonite saturated with pure- or salt-water by the method of unified molecular dynamics and homogenization analysis. Eng Geol 2001;60(1–4):127–38. http://dx.doi.org/10.1016/S0013-7952(00)00095-8.
[33] Ichikawa Y, Kawamura K, Fujii N, Nattavut T. Molecular dynamics and multiscale homogenization analysis of seepage/diffusion problem in bentonite clay. Int J Numer Meth Eng 2002;54(12):1717–49.
[34] Ichikawa Y, Kawamura K, Fujii N, Nattavut T. Molecular simulation and multiscale homogenization analysis for microinhomogeneous clay materials. Eng Comput 2003;20(5–6):559–82.
[35] Ichikawa Y, Kawamura K, Theramast N, Kitayama K. Secondary and tertial consolidation of bentonite clay: consolidation test, molecular dynamics simulation and multiscale homogenization analysis. Mech Mater 2004;36(5–6):487–513. http://dx.doi.org/10.1016/S0167-6636(03)00073-5.
[36] Song CR, Cho H, Jung YH, Cheng AHD, Alostaz A. Bridging molecular, particulate, and continuum mechanics for geomechanics application. Adv Meas Model Soil Behav 2007:1–10. http://dx.doi.org/10.1061/40917(236)33.
[37] Bourg IC, Sposito G. Connecting the molecular scale to the continuum scale for diffusion processes in smectite-rich porous media. Environ Sci Technol 2010;44(6):2085–91.
[38] Bourg IC, Sposito G. Molecular dynamics simulations of the electrical double layer on smectite surfaces contacting concentrated mixed electrolyte (NaCl–CaCl 2) solutions. J Colloid Interface Sci 2011;360(2):701–15.
[39] Katti DR, Schmidt SR, Ghosh P, Katti KS. Modeling the response of pyrophyllite interlayer to applied stress using steered molecular dynamics. Clays Clay Miner 2005;53(2):171–8.
[40] Katti DR, Ghosh P, Schmidt S, Katti KS. Mechanical properties of the sodium montmorillonite interlayer intercalated with amino acids. Biomacromolecules 2005;6(6):3276–82.
[41] Katti DR, Schmidt SR, Ghosh P, Katti KS. Molecular modeling of the mechanical behavior and interactions in dry and slightly hydrated sodium montmorillonite interlayer. Can Geotech J 2007;44(4):425–35.
[42] Katti DR, Srinivasamurthy L, Katti KS. Molecular modeling of initiation of interlayer swelling in Na-montmorillonite expansive clay. Can Geotech J 2015;52(9):1385–95.
[43] Amarasinghe PM, Anandarajah A. Influence of fabric variables on clay–water–air capillary meniscus. Can Geotech J 2011;48(7):987–95.
[44] Anandarajah A, Amarasinghe PM. Microstructural investigation of soil suction and hysteresis of fine-grained soils. J Geotech Geoenviron Eng 2011;138(1):38–46.
[45] Liu WK, Karpov EG, Zhang S, Park HS. An introduction to computational nanomechanics and materials. Comput Methods Appl Mech Eng 2004;193(17–20):1529–78. http://dx.doi.org/10.1016/j.cma.2003.12.008.
[46] Li S, Wang G. Introduction to micromechanics and nanomechanics. World Scientific; 2008 [ISBN 9789812814135].
[47] Rapaport D. The art of molecular dynamics simulation. Place: Cambridge University Press; 2004 [ISBN 9780521825689].
[48] Cygan RT, Liang JJ, Kalinichev AG. Molecular models of hydroxide, oxyhydroxide, and clay phases and the development of a general force field. J Phys Chem B 2004;108(4):1255–66.
[49] Hockney R, Eastwood J. Computer simulation using particles. CRC Press; 1988 [ISBN 9781439822050].
[50] Mitchell J, Soga K. Fundamentals of soil behavior. John Wiley & Sons; 2005 [ISBN 9780471463023].
[51] Levien L, Prewitt CT, Weidner DJ. Structure and elastic properties of quartz at pressure. Am Mineral 1980;65(9–10):920–30.
[52] Tseng HY, Heaney PJ, Onstott TC. Characterization of lattice strain-induced by neutron-irradiation. Phys Chem Miner 1995;22(6):399–405.
[53] Richardson SM, Richardson JW. Crystal structure of a pink muscovite from Archer's Post, Kenya; implications for reverse pleochroism in dioctahedral micas. Am Mineral 1982;67:69–75.
[54] Lopes PEM, Murashov V, Tazi M, Demchuk E, MacKerell AD. Development of an empirical force field for silica. Application to the quartz–water interface. J Phys Chem B 2006;110(6):2782–92. http://dx.doi.org/10.1021/jp055341i.
[55] Skelton AA, Fenter P. Simulations of the quartz (1011)/water interface: a comparison of classical force fields, ab initio molecular dynamics, and X-ray reflectivity experiments. J Phys Chem C 2011:2076–88.
[56] Kerisit S, Liu CX, Ilton ES. Molecular dynamics simulations of the orthoclase (001)- and (010)-water interfaces. Geochim Cosmochim Acta 2008;72(6):1481–97. http://dx.doi.org/10.1016/j.gca.2007.12.014.
[57] Teich-McGoldrick SL, Greathouse JA, Cygan RT. Molecular dynamics simulations of structural and mechanical properties of muscovite: pressure and temperature effects. J Phys Chem C 2012;116(28):15099–107. http://dx.doi.org/10.1021/jp303143s.
[58] Allen P, Tildesley D. Computer simulation of liquids. Clarendon Press; 1989 [ISBN 9780198556459].
[59] Berendsen HJ, Postma JP, van Gunsteren WF, Hermans J. In: Interaction models for water in relation to protein hydration. Springer; 1981. p. 331–42 [ISBN 9048183685].
[60] Berendsen HJC, Grigera JR, Straatsma TP. The missing term in effective pair potentials. J Phys Chem 1987;91(24):6269–71.
[61] Jorgensen WL, Chandrasekhar J, Madura JD, Impey RW, Klein ML. Comparison of simple potential functions for simulating liquid water. J Chem Phys 1983;79(2):926–35. http://dx.doi.org/10.1063/1.445869.
[62] Martínez L, Andrade R, Birgin EG, Martínez JM. PACKMOL: a package for building initial configurations for molecular dynamics simulations. J Comput Chem 2009;30(13):2157–64. http://dx.doi.org/10.1002/jcc.21224.
[63] Cho GC, Santamarina JC. Unsaturated particulate materials–particle-level studies. J Geotech Geoenviron Eng 2001.
[64] Leroch S, Wendland M. Influence of capillary bridge formation onto the silica nanoparticle interaction studied by grand canonical monte carlo simulations. Langmuir 2013;29(40):12410–20.
[65] Plimpton S. Fast parallel algorithms for short-range molecular-dynamics. J Comput Phys 1995;117(1):1–19. http://dx.doi.org/10.1006/jcph.1995.1039.
[66] Plimpton S, Crozier P, Thompson A. LAMMPS-large-scale atomic/molecular massively parallel simulator. Sandia National Laboratories 2007;18.
[67] Humphrey W, Dalke A, Schulten K. VMD: visual molecular dynamics. J Mol Graph 1996;14(1):33–8 (27).
[68] Ryckaert JP, Ciccotti G, Berendsen HJ. Numerical integration of the cartesian equations of motion of a system with constraints: molecular dynamics of n-alkanes. J Comput Phys 1977;23(3):327–41.
[69] Szyszka D. Study of contact angle of liquid on solid surface and solid on liquid surface. Prace Naukowe Instytutu Górnictwa Politechniki Wrocławskiej 2012:131–46.
[70] Karagüzel C, Can MF, Sönmez E, Celik MS. Effect of electrolyte on surface free energy components of feldspar minerals using thin-layer wicking method. J Colloid Interface Sci 2005;285(1):192–200.